Nuclear Medicine and Biology 124-125 (2023) 108384

Contents lists available at ScienceDirect

Nuclear Medicine and Biology

journal homepage: www.elsevier.com/locate/nucmedbio

Evaluation of affinity matured Affibody molecules for imaging of the immune checkpoint protein B7-H3☆

Maryam Oroujeni [a,b,*,1], Ekaterina A. Bezverkhniaia [c,d,e,1], Tianqi Xu [a], Yongsheng Liu [a], Evgenii V. Plotnikov [c], Susanne Klint [b], Eva Ryer [b], Ida Karlberg [b], Anna Orlova [c,e], Fredrik Y. Frejd [a,b], Vladimir Tolmachev [a,c,*]

[a] Department of Immunology, Genetics and Pathology, Uppsala University, 751 85 Uppsala, Sweden
[b] Affibody AB, 171 65 Solna, Sweden
[c] Research Centrum for Oncotheranostics, Research School of Chemistry and Applied Biomedical Sciences, Tomsk Polytechnic University, 634050 Tomsk, Russia
[d] Scientific and Research Laboratory of Chemical and Pharmaceutical Research, Siberian State Medical University, Tomsk 634050, Russia
[e] Department of Medicinal Chemistry, Uppsala University, 751 83 Uppsala, Sweden

ARTICLE INFO

Keywords:
B7-H3
Affibody molecule
Affinity maturation
Peptide-based cysteine-containing chelator –GGGC
AC12-GGGC
Technetium-99m (^{99m}Tc)
SKOV-3 xenograft
SPECT/CT imaging

ABSTRACT

B7-H3 (CD276), an immune checkpoint protein, is a promising molecular target for immune therapy of malignant tumours. Sufficient B7-H3 expression level is a precondition for successful therapy. Radionuclide molecular imaging is a powerful technique for visualization of expression levels of molecular targets *in vivo*. Use of small radiolabelled targeting proteins would enable high-contrast radionuclide imaging of molecular targets if adequate binding affinity and specificity of an imaging probe could be provided. Affibody molecules, small engineered affinity proteins based on a non-immunoglobulin scaffold, have demonstrated an appreciable potential in radionuclide imaging. Proof-of principle of radionuclide visualization of expression levels of B7-H3 *in vivo* was demonstrated using the [^{99m}Tc]Tc-AC12-GGGC Affibody molecule. We performed an affinity maturation of AC12, enabling selection of clones with higher affinity. Three most promising clones were expressed with a –GGGC (triglycine-cysteine) chelating sequence at the C-terminus and labelled with technetium-99m (^{99m}Tc). ^{99m}Tc-labelled conjugates bound to B7-H3-expressing cells specifically *in vitro* and *in vivo*. Biodistribution in mice bearing B7-H3-expressing SKOV-3 xenografts demonstrated improved imaging properties of the new conjugates compared with the parental variant [^{99m}Tc]Tc-AC12-GGGC. [^{99m}Tc]Tc-SYNT-179 provided the strongest improvement of tumour-to-organ ratios. Thus, affinity maturation of B7-H3 Affibody molecules could improve biodistribution and targeting properties for imaging of B7-H3-expressing tumours.

1. Introduction

B7-H3 (B7 homolog 3 or CD276), a 316 amino-acid long transmembrane glycoprotein, belongs to the B7 ligand family of immune checkpoint molecules. This protein is involved in oncogenic signalling, tumour cell plasticity, and drug resistance. It has protumourigenic actions, such as facilitating migration and invasion, chemoresistance, endothelial-to-mesenchymal transition, angiogenesis and affecting tumour cell metabolism [1]. B7-H3 is overexpressed with high frequency in many different cancer types *e.g.* neuroblastoma [2], melanoma [3], glioblastoma [4], non-small cell lung cancer [5], pancreatic [6,7], breast [8], prostate [9,10] and ovarian cancers [11], whereas its expression in most normal organs and tissues is low [12]. Remarkably, B7-H3 overexpression is associated with an aggressive cancer phenotype in some cancer types resulting in an increased risk of cancer recurrence, cancer metastases, poor prognosis and resistance in patients

☆ This is a free access article and can be viewed on the journal's Web site (www.nucmedbio.com). Complimentary access to this article is available until the next issue publishes online.

* Corresponding authors at: Department of Immunology, Genetics and Pathology, Uppsala University, 751 85 Uppsala, Sweden.
E-mail addresses: maryam.oroujeni@igp.uu.se (M. Oroujeni), ekaterina.bezverkhniaia@ilk.uu.se (E.A. Bezverkhniaia), tianqi.xu@igp.uu.se (T. Xu), susanne.klint@affibody.se (S. Klint), eva.ryer@affibody.se (E. Ryer), ida.karlberg@affibody.se (I. Karlberg), anna.orlova@ilk.uu.se (A. Orlova), fredrik.frejd@affibody.se (F.Y. Frejd), vladimir.tolmachev@igp.uu.se (V. Tolmachev).
[1] Contributed equally to the work.

https://doi.org/10.1016/j.nucmedbio.2023.108384
Received 30 June 2023; Received in revised form 25 August 2023; Accepted 30 August 2023
Available online 1 September 2023

[9,10,13–16]. Taking this into account, utilizing the immune checkpoint molecule B7-H3 as a target for diagnosis, prognosis, and/or treatment applications would be rational.

Visualization of overexpression of cell-surface proteins in malignant cells enables stratification of patients for specific therapies. Analysis of biopsy samples is the commonly used method to determine the expression level of many molecular targets in solid tumours. However, the use of biopsies is associated with several limitations because of the invasive nature of collecting them. Radionuclide molecular imaging using single-photon emission computed tomography (SPECT) and/or positron-emission tomography (PET) [17] could be used as a non-invasive technique to estimate B7-H3 expression level enabling personalization of anti-cancer treatment.

Some radiolabelled antibody-based probes for targeting B7-H3-expressing tumours have been developed recently. A specific tumour localisation, and acceptable safety of these probes in preclinical models and phase I clinical trials in patients have been demonstrated [18–21]. However, slow extravasation rate in tumour and the slow clearance from blood circulation and non-targeted organs are the foremost disadvantages of the use of monoclonal antibodies for imaging. These features result in low imaging contrast (even several days after injection) and an elevated dose burden to the patient [22–24]. Reduction of the size of targeting probes would be an alternative to overcome the issues associated with the use of monoclonal antibodies for imaging. The Affibody molecule, a 58-amino acid cysteine-free scaffold, is an engineered affinity protein (with the size of 6–7 kDa), which can be produced either recombinantly in bacteria or by chemical synthesis. Robust structure, straightforward production procedures, high affinity and site-specific radiolabelling are advantages of Affibody molecules compared to antibodies [25] making them attractive imaging agents for visualization of different molecular targets. Importantly, they have shown high extravasation rate in tumours and fast clearance from blood and non-targeted organs resulting in a high imaging contrast and the optimal imaging time of a few hours after injection [26]. Affibody-based tracers have been developed for preclinical imaging of different molecular targets, such as HER1/EGFR [27,28], HER2 [29,30], HER3 [31], PDGFRß [32], IGF-1R [33], and CAIX [34]. Early stage clinical trials demonstrated advantageous biodistribution and safety of HER2-targeting Affibody molecules [35,36]. Furthermore, the data from these studies suggested a capability of Affibody molecules for high-contrast imaging of breast cancer with high HER2 expression and prediction of tumour response to HER2-targeted therapy [37]. This indicates that Affibody molecules could be a promising class of imaging agents. Thus, it would be desirable to develop Affibody-based imaging agents for visualization the B7-H3-expressing tumours.

A precondition for successful translation of a radionuclide molecular imaging agent into clinic use is high sensitivity provided by the imaging agent, which depends on contrast (determined by the ratio of radioactivity concentrations in the tumour and in surrounding healthy tissues, so-called tumour-to-organ ratio). Thus, for development of new imaging agents, the focus should be on factors increasing the tumour-to-organ ratio. This could be possible by both increasing tumour uptake of radioactivity and by decreasing uptake in healthy tissues. Several factors can influence tumour-to-organ ratio. Affinity is one of the crucial factors defining the efficacy of tumour targeting. Internalization of Affibody molecules is relatively slow, typically around 20–30 % of cell-bound conjugate per day, and in this case, cellular retention of radioactivity results from the strong target binding [38,39]. Several studies have been performed to investigate the influence of binding strength (affinity) of targeting agents on their tumour targeting [40–43]. Some studies have demonstrated that affinity maturation can be used as a key technique to improve affinity and binding interactions of Affibody molecules targeting different molecular targets, such as EGFR/HER1 [44], HER2 [29], HER3 [45] and PDGFRβ [46].

The feasibility of preclinical imaging of B7-H3-expressing tumours at the day of injection using the radiolabelled AC12 Affibody molecule with nanomolar affinity was demonstrated recently [47]. We found that the expression level of B7-H3 is 45,000–60,000 molecules per cell. It should be noted that accumulation and retention of radioactivity in a tumour with such level of target expression would need a subnanomolar affinity of an Affibody molecule [43]. Increasing the affinity of B7-H3 targeted Affibody molecules would be desirable to obtain higher radioactivity accumulation and retention in tumour and improve imaging contrast. The aim of this study was to test the hypothesis that affinity matured B7-H3-binding Affibody molecules could improve targeting properties of Affibody molecules for imaging of B7-H3-expressing tumours. *In vitro* experiments (specificity and affinity) were performed using B7-H3-expressing cells. To obtain more reliable data, a head-to-head biodistribution of the affinity matured Affibody binders and the parental variant AC12 (both labelled with ^{99m}Tc) was studied in mice bearing B7-H3-expressing SKOV-3 xenografts. Uptake in B7-H3-negative Ramos xenografts was used as a specificity control. SPECT/CT imaging of these new binders was performed.

2. Materials and methods

2.1. General

Most of the chemicals used in this study were purchased from Sigma-Aldrich, Sweden AB. ^{99m}Tc was obtained as pertechnetate by elution of an Ultra TechneKow generator (Mallinckrodt, Petten, The Netherlands) in sterile 0.9 % sodium chloride (Mallinckrodt, Petten, the Netherlands). The Cyclone Storage Phosphor system (Perkin-Elmer, Wellesley, MA, USA) was used for quantitative measurement of radioactivity distribution in instant thin-layer chromatography strips. The radioactivity from cells and animal samples was measured using an automated gamma-spectrometer equipped with a 3-inch NaI (TI) well detector (2480 Wizard, Wallac, Turku, Finland). Radioactivity for labelling and injection formulation was measured using a dose calibrator VDC-405 (Veenstra Instruments BV, Joure, The Netherlands) equipped with an ionization chamber.

In vitro cell studies were performed using the B7-H3-expressing ovarian cancer SKOV-3 and breast cancer BT-474 cell lines, purchased from the American Type Culture Collection (ATCC). B7-H3-negative xenografts were established using Ramos lymphoma cells (from ATCC). Cells were cultured in Roswell Park Memorial Institute (RPMI) 1640 medium (Sigma-Aldrich), supplemented with 10 % (SKOV-3) or 20 % (BT-474) fetal bovine serum (FBS), 2 mM L-glutamine, 100 IU/mL penicillin and 100 mg/mL streptomycin.

In vitro studies and biodistribution data were analysed by unpaired 2-tailed *t*-test and one-way ANOVA using GraphPad Prism (version 6 for Windows; GraphPad Software) to determine significant differences ($p < 0.05$).

2.2. Affinity maturation, production and characterization of anti-B7-H3 Affibody binders

A maturation library based on AC12 was designed to further assess the sequence space to gain binders with increased affinity and improved properties. Phage display selection followed by characterization of a large set of matured binders resulted in selection of lead B7-H3-binding Affibody molecules for further evaluation.

Three affinity matured Affibody molecules denoted SYNT-177, SYNT-179 and SYNT-181 as well as the reference molecule AC12-GGGC were produced by solid phase peptide synthesis using the Fmoc/tBu strategy. The synthesized Affibody molecules were purified by preparative reversed phase high-performance liquid chromatography, followed by buffer exchanged to an acetate-containing buffer and finally lyophilized in aliquots of 3–4 mg. The lyophilized Affibody molecules were stored at −20 °C. This work was performed as fee-for-service by the contract manufacturer Bachem (St Helens, UK).

For the radiolabelling, the lyophilized Affibody molecules were

weighed and dissolved in PBS (Corning, Glendale, AZ, USA) supplemented with 2 mM EDTA (Corning, Glendale, AZ, USA) to a final concentrations of 2.0 mg/mL of the Affibody molecule, taken the specified peptide contents in consideration. The solubilized Affibody molecules were aliquoted in 50 μL aliquots (100 μg) and stored at −80 °C.

The purity of the Affibody molecules SYNT-177, SYNT-179, SYNT-181 and AC12-GGGC were determined by reversed phase ultra-high-performance liquid chromatography (RP-UPLC), as previously described [47].

Characterization of the B7-H3-binding Affibody molecules were made following the same protocols previously described for AC12-GGGC [47]. Circular Dichroism (CD) analysis was used to determine the molecules melting temperature (T_m), and to analyse secondary structure and refolding after thermal denaturation. IEF gel analysis was performed to determine the isoelectric point (pI) of the molecules.

The Affibody molecules SYNT-177, SYNT-179, SYNT-181 and the reference molecule AC12-GGGC were tested in terms of binding to B7-H3 expressing SKOV-3 cells. The cells were placed in a V-bottom 96-well plate (0.2×10^6 cells/well) and incubated at 4 °C for 1 h with Affibody molecules at decreasing concentrations from 500 nM to 32 pM. After 1× washing in PBS with 1 % fetal bovine serum (FBS), binding of Affibody molecules was identified by an anti-Affibody polyclonal antibody (4 μg/mL) and incubated at 4 °C for 1 h followed by an Alexa488 conjugated goat-anti-rabbit IgG diluted 1:2000 and incubated at 4 °C for 1 h. After 2× washing in PBS with 1 % FBS, fluorescence intensity was measured by a multimode plate reader (Enspire). Each sample was tested in quadruplicates. Binding curves were plotted and EC50 values were determined using software GraphPad Prism.

2.3. Radiolabelling and in vitro stability

Affibody molecules were site-specifically labelled with ^{99m}Tc using a lyophilized kit, as described earlier [48]. A freeze-dried labelling kit containing 75 μg of tin (II) chloride dihydrate (Fluka Chemika, Buchs, Switzerland), 100 μg of ethylenediaminetetraacetic acid tetra sodium salt ($EDTANa_4$) (Sigma-Aldrich, Munich, Germany) and 5 mg of gluconic acid sodium salt (Celsus Laboratories, Geel, Belgium) was prepared for labelling with ^{99m}Tc. Radiolabelling was performed by following procedure: the content of a freeze-dried kit dissolved in 120-μL degassed PBS, was added to 100 μg of the Affibody molecule. 80 μL (200–300 MBq) of ^{99m}Tc-pertechnetate was added to the reaction mixture followed by degassing to protect the mixture from oxidation. The reaction mixture was incubated at 90 °C for 60 min. Radiochemical yield was analysed using instant thin layer chromatography (ITLC-SG) (Agilent Technologies, Santa Clara, CA, USA) using PBS as the mobile phase (Affibody: Rf = 0.0, other forms of ^{99m}Tc: Rf = 1.0). The reduced hydrolysed technetium colloid (RHT) percentage in the product was measured using pyridine:acetic acid:water (10:6:3) mixture as the mobile phase (^{99m}Tc colloid: Rf = 0.0, other forms of ^{99m}Tc and radiolabelled affibody molecule: Rf = 1.0). Radiochemical yield was over 95 % for all conjugates. Thus, no further purification was performed for *in vitro* and *in vivo* experiments.

A reverse phase-HPLC conducted on an Elite LaChrom system (Hitachi, VWR, Darmstadt, Germany) consisting of an L-2130 pump, a UV detector (L-2400), and a radiation flow detector (Bioscan, Washington, DC, USA) coupled in series was used to cross-validate ITLC results. Purity of non-labelled and ^{99m}Tc-labelled compounds was analysed using an analytical column (Vydac RP C18 column, 300 Å; 3 × 150 mm; 5 μm). HPLC conditions were as follows: A = 10 mM TFA/H_2O, B = 10 mM TFA/acetonitrile, UV-detection at 220 nm, gradient elution: 0–15 min at 5 % to 70 % B, 15–18 min at 70 % to 95 % B, 19–20 min at 5 % B, and a flow rate was 1.0 mL/min.

In vitro stability was performed by incubating the fractions of the freshly ^{99m}Tc-labelled conjugate (10 μL, 4 μg) with excess amount of PBS (40 μL) for at 37 °C for 60 min. The test was performed in triplicates. The release of ^{99m}Tc was monitored by ITLC-SG as described above.

2.4. In vitro studies

For *in vitro* studies, B7-H3-expressing cells, ovarian carcinoma SKOV-3 and breast carcinoma BT-474 cell lines, were used. B7-H3 expression levels were estimated to be 68,000 and 45,000 receptors per cell for SKOV-3 and BT-474, respectively [47]. Cells (10^6 cells/dish) were seeded in cell-culture dishes (35 mm in diameter). A set of three dishes was used for *in vitro* binding specificity.

Binding specificity of ^{99m}Tc-labelled Affibody molecules was performed by following procedure: Cells in three blocked dishes were presaturated with 200-fold excess of non-labelled Affibody molecule 15 min before adding the labelled conjugate. Then, the cells in both blocked and nonblocked dishes were incubated with a labelled conjugate (10 nM) in a humidified incubator (5 % CO_2, 37 °C) for 1 h. The medium was discarded, the cells were washed with cold serum-free medium (2 mL). Trypsin–EDTA solution (0.5 mL per dish) was added, and cells were incubated for 10–15 min. Detached cells were resuspended and collected with 0.5 mL of complete medium in fraction tubes. The radioactivity of cells was measured using an automated gamma counter and the cell-bound radioactivity was calculated.

Kinetics of binding to, dissociation of ^{99m}Tc-labelled Affibody molecules from B7-H3-expressing SKOV-3 cells and affinity were measured using LigandTracer Yellow instrument (Ridgeview Instruments AB, Vänge, Sweden), as previously described [49]. Cells were seeded on a local area of a cell culture dish (89 mm in diameter, Nunclon™, NUNC A/S, Roskilde, Denmark) one day before the experiment. The measurements were performed at room temperature to prevent internalization. Association curves were recorded at 1 and 3 nM of ^{99m}Tc-labelled conjugates. Thereafter, the radioactive medium was discarded and replaced with fresh non-radioactive medium, and the dissociation curves were recorded for several hours. The data were analysed using the InteractionMap software (Ridgeview Diagnostics AB, Uppsala, Sweden) to calculate the association rate, the dissociation rate, and the dissociation constant at equilibrium (K_D). Experiment was performed in duplicates. The basics of the InteractionMap analysis was previously described [50].

2.5. In vivo studies

Animal experiments were performed in accordance with the national legislation for work with laboratory animals. Approval was permitted by the Ethical Committee for Animal Research in Uppsala (ethical permission C4/16, decision from 26 February 2016). Four mice per data point were used for biodistribution experiments.

Biodistribution and targeting properties of ^{99m}Tc-labelled Affibody conjugates were evaluated in BALB/C nu/nu mice bearing B7-H3-positive SKOV-3 xenografts and compared directly with the parental variant [^{99m}Tc]Tc-AC12-GGGC. To establish xenografts, SKOV-3 cells (10^7 cells/mouse) were subcutaneously injected on the right hind leg of female BALB/c nu/nu mice. B7-H3-negative Ramos cells (5×10^6 cells/mouse) were used to test *in vivo* specificity. Cells were subcutaneously implanted on the left hind leg of female BALB/c nu/nu in mice. The experiments were performed three weeks after the implantation. The average animal weight was 19.1 ± 1.9 g. The average tumour weight was 0.10 ± 0.08 g and 0.09 ± 0.07 g for SKOV-3 and Ramos xenografts, respectively. The biodistribution was measured 4 h after injection in mice bearing SKOV-3 xenografts. Groups of four mice were injected with ^{99m}Tc-labelled Affibody molecules (3 μg, 60 kBq, 100 μL in PBS) into the tail vein. After 4 h, mice were euthanized by overdosing of anaesthetic solution (20 μL of solution per gram of body weight: ketamine, 10 mg/mL; xylazine, 1 mg/mL) followed by a heart puncture. Blood, organs and tissues were collected and weighed. The organ radioactivity was measured using a gamma spectrometer along with three standards and empty syringes for each animal. Uptake values for organs were calculated as the percentage-injected dose per gram tissue (%ID/g). Lower GI tract organs, such as the large intestine and cecum, were excised with their content and their activity was measured to estimate activity

excreted *via* bile. To test B7-H3-specific accumulation *in vivo*, one group of animals bearing B7-H3-negative Ramos xenografts was injected with the same peptide and activity doses for the best variant and the biodistribution was measured 4 h after injection. Biodistribution of the best variant, [^{99m}Tc]Tc-SYNT-179, was studied at 2 and 4 h after injection. The biodistribution measurements were performed in the same way as described above.

A small animal SPECT/CT imaging was performed to confirm biodistribution results. One SKOV-3 bearing mice was intravenously injected with ^{99m}Tc-labelled Affibody molecule (6 MBq/3 μg per mouse) for each variant. To confirm *in vivo* specificity, one mouse bearing B7-H3-negative Ramos xenograft was intravenously injected with the same peptide and activity doses as mentioned above. The mice were imaged 4 h after injection using a nanoScan SPECT/CT scanner (Mediso Medical Imaging Systems, Budapest, Hungary). The mice were euthanized by CO_2 asphyxiation immediately before being placed in the camera. The computed tomography (CT) acquisition was carried out at the following parameters: energy peak of 50 kV, 670 μA, 480 projections, and 2.29-min acquisition time. SPECT acquisition was performed at the following parameters: ^{99m}Tc energy peak of 140 keV, window width of 20 %, matrix of 256 × 256, and acquisition time of 1 h. CT images were reconstructed in real-time using Nucline 2.03 Software (Mediso Medical Imaging Systems, Budapest, Hungary). SPECT raw data were reconstructed using TeraTomo™ 3D SPECT reconstruction technology.

3. Results

3.1. Characterization of anti-B7-H3 Affibody molecules

The lyophilized Affibody molecules SYNT-177, SYNT-179, SYNT-181 and AC12-GGGC (Fig. 9) were dissolved in PBS supplemented with 2 mM EDTA. Purity was determined by RP-UPLC and the isoelectric points (pI) were determined with isoelectric focusing gel electrophoresis analysis (Table 1).

Circular dichroism (CD) analysis showed that each B7-H3 binding Affibody molecule had an α-helix secondary structure and refolded with maintained overall structure after thermal denaturation. The melting temperatures (T_m) were determined (Table 1).

The synthesized Affibody molecules were tested in terms of binding to B7-H3 expressing SKOV-3 cells. Binding curves were plotted and are shown in Fig. 1. EC_{50} values were determined using the software GraphPad Prism and are shown in Table 2. The matured Affibody molecules showed 3–4 times better binding capacity compared to AC12-GGGC.

3.2. Radiolabelling and in vitro stability

Anti-B7-H3 Affibody molecules were successfully labelled with ^{99m}Tc (Table 3). Since the radiochemical yield was ≥95 %, and RHT was ≤5 %, the labelled conjugates were used without further purification for *in vitro* and *in vivo* studies. The specific activity of ^{99m}Tc-labelled conjugates was 3–6 MBq/μg. ^{99m}Tc-labelled conjugates were stable during incubation at 37 °C for 1 h in the presence of excess of phosphate-buffered saline (PBS). No release of ^{99m}Tc from the radioconjugates was observed.

Table 1
Determined purity, isoelectric point (pI) and melting temperature (Tm) of produced Affibody molecules.

Construct	RP-UPLC purity, %	pI	T_m, °C
SYNT-177	92	6.8	56
SYNT-179	91	4.7	50
SYNT-181	97	7.7	57
AC12-GGGC	92	4.7	55

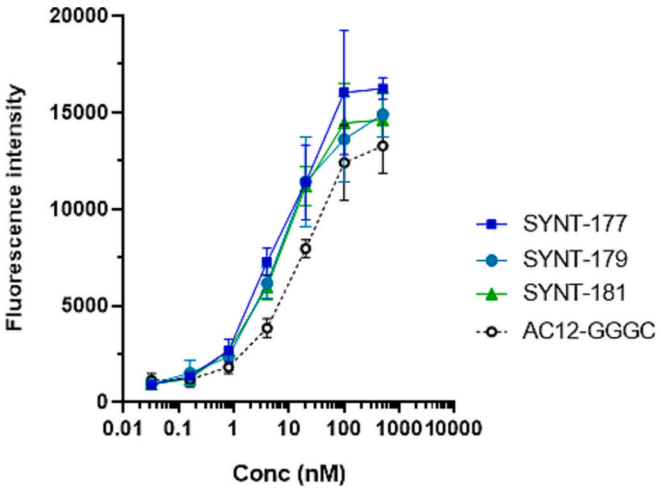

Fig. 1. Binding of Affibody molecules to B7-H3 expressing SKOV-3 cells.

Table 2
EC_{50} determination from SKOV-3 cell binding.

	SYNT-177	SYNT-179	SYNT-181	AC12-GGGC
EC_{50} (nM)	5.7	7.5	7.6	22.0

Table 3
Labelling of Affibody molecules with ^{99m}Tc and *in vitro* stability.

Construct	Radiochemical yield, %	Stability in PBS, 37 °C, 1 h
SYNT-177	96 ± 2	98 ± 1
SYNT-179	95 ± 4	97 ± 1
SYNT-181	95 ± 3	98 ± 1
AC12-GGGC[a]	96 ± 2	96 ± 1

[a] AC12-GGGC was chosen as a reference variant.

Radio-HPLC analysis was performed to cross-validate the radio-iTLC results. According to radio-HPLC chromatograms (Fig. 2), the retention time of ^{99m}Tc-labelled conjugates was around 11–12 min. Only one major peak was observed, corresponding to radiolabelled Affibody molecule.

3.3. In vitro studies

In vitro B7-H3-binding specificity test of ^{99m}Tc-labelled conjugates showed that the binding was significantly ($p < 5 \times 10^{-5}$) decreased when the cells were pre-saturated with an excess amount of non-labelled anti-B7-H3 Affibody molecules (Fig. 3) before adding the labelled one.

The kinetics of interaction of ^{99m}Tc-labelled conjugates to SKOV-3 cells was studied in real-time using a LigandTracer Yellow instrument. The results are presented in Fig. 4 and Table 4. According to LigandTracer measurements and InteractionMap calculations, the best fit of the binding of the three radioconjugates to SKOV-3 cell line was achieved using a 1:2 model, suggesting that there were two types of interactions with B7-H3 target. [^{99m}Tc]Tc-SYNT-179 showed the lowest K_{D1} value in subnanomolar range ($K_{D1} = 0.028 \pm 0.001$ nM, % weight = 12) and the more abundant K_{D2} value was 8.2 ± 0.5 nM, % weight = 88. The corresponding equilibrium dissociation constants (K_D) values for all radioconjugates are shown in Table 4.

3.4. In vivo studies

The results of the biodistribution of ^{99m}Tc-labelled Affibody molecules compared to the reference variant [^{99m}Tc]Tc-AC12-GGGC in mice bearing B7-H3-expressing xenografts 4 h after injection are presented in

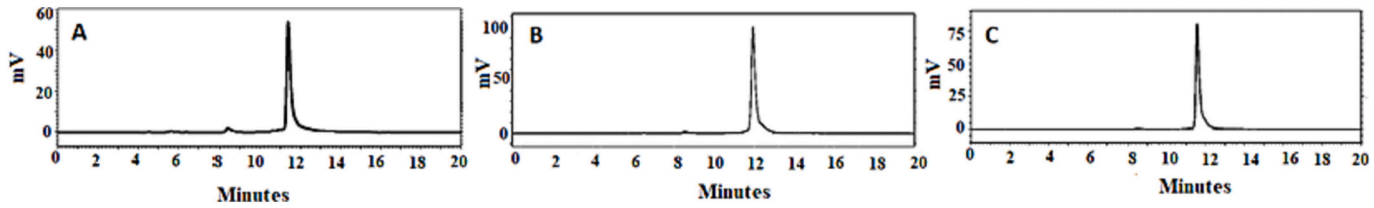

Fig. 2. Reversed-phase radio-HPLC chromatograms of ^{99m}Tc-labelled (A) SYNT-177, (B) SYNT-179 and (C) SYNT-181 Affibody molecules. The retention times (Rt) are expressed in minutes.

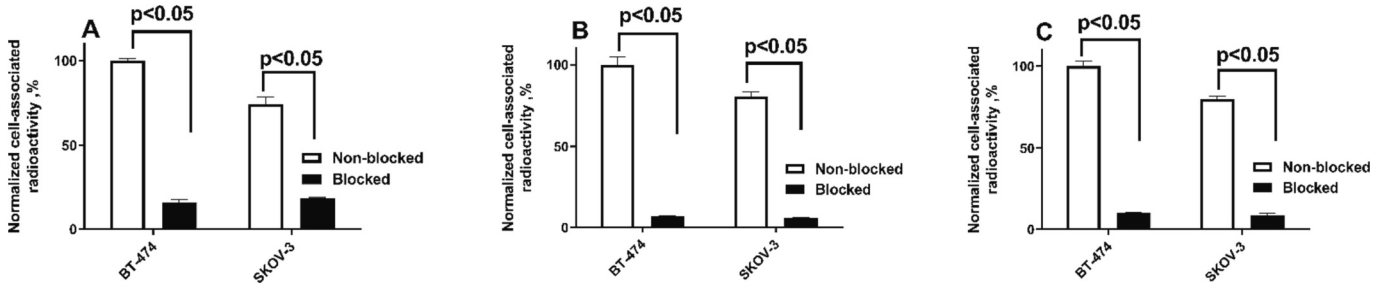

Fig. 3. *In vitro* binding specificity of (A) [^{99m}Tc]Tc-SYNT-177, (B) [^{99m}Tc]Tc-SYNT-179 and (C) [^{99m}Tc]Tc-SYNT-181 on B7-H3-expressing SKOV-3 and BT-474 cells. Data are normalized to the average value of cell-associated radioactivity for non-blocked samples of BT-474 cell line for each variant. The data are presented as an average value from three samples ± SD.

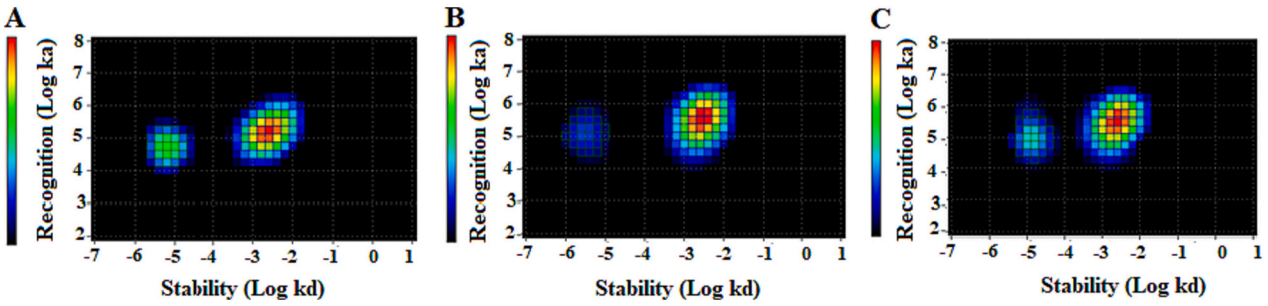

Fig. 4. InteractionMap results for (A) [^{99m}Tc]Tc-SYNT-177, (B) [^{99m}Tc]Tc-SYNT-179 and (C) [^{99m}Tc]Tc-SYNT-181 binding to SKOV-3 cells. Data were obtained from LigandTracer measurement of cell-bound activity during association of labelled conjugate to and dissociation from SKOV-3 cells. Measurements were performed in duplicates.

Table 4
Dissociation constants at equilibrium (K_D) for the interaction between ^{99m}Tc-labelled Affibody molecules and B7-H3-expressing SKOV-3 cells determined using an InteractionMap analysis.

	K_{D1} (nM)	Weight$_1$ (%)	K_{D2} (nM)	Weight$_2$ (%)
SYNT-177	0.121 ± 0.006	27	13 ± 3.4	73
SYNT-179	0.028 ± 0.001	12	8.2 ± 0.5	88
SYNT-181	0.138 ± 0.004	21	8.2 ± 0.4	79
AC12-GGGC[a]	1.9 ± 0.8	23	68.8 ± 7.4	67

[a] Data for AC12-GGGC has been taken from reference [47].

Table 5. Biodistribution data demonstrated that [^{99m}Tc]Tc-SYNT-179 has the lowest blood concentration (0.06 ± 0.01 %ID/g), which was significantly ($p < 0.05$) lower than for [^{99m}Tc]Tc-SYNT-181 (0.13 ± 0.03 %ID/g). Tumour uptake was significantly ($p < 0.05$) higher for [^{99m}Tc]Tc-SYNT-181 (3.19 ± 0.21 %ID/g) compared to [^{99m}Tc]Tc-SYNT-179 (1.54 ± 0.19 %ID/g) and [^{99m}Tc]Tc-AC12-GGGC (1.04 ± 0.08 %ID/g). Importantly, hepatic uptake of [^{99m}Tc]Tc-SYNT-179 (0.26 ± 0.02 %ID/g) was significantly ($p < 0.05$) lower than for the other radioconjugates (2.82 ± 0.56, 1.27 ± 0.31 and 2.57 ± 0.42 %ID/g for [^{99m}Tc]Tc-SYNT-177, [^{99m}Tc]Tc-SYNT-181 and [^{99m}Tc]Tc-AC12-GGGC, respectively). [^{99m}Tc]Tc-SYNT-181 showed significantly ($p < 0.05$) lower renal uptake (5.85 ± 0.28 %ID/g) compared to [^{99m}Tc]Tc-SYNT-179 (10.37 ± 1.34 %ID/g) and [^{99m}Tc]Tc-AC12-GGGC (10.30 ± 1.13 %ID/g). Uptake in bone was significantly ($p < 0.05$) lower for [^{99m}Tc]Tc-SYNT-179 (0.006 ± 0.001 %ID/g) compared to other conjugates.

The tumour-to-organ ratios are provided in Table 6. Tumour-to-salivary gland, tumour-to-liver and tumour-to-spleen ratios were significantly ($p < 0.05$) higher for [^{99m}Tc]Tc-SYNT-179 compared to those for other variants. Significantly ($p < 0.05$) higher tumour-to-blood ratio for [^{99m}Tc]Tc-SYNT-179 (25.7 ± 2.5) compared to [^{99m}Tc]Tc-SYNT-177 (11.3 ± 4.2) and [^{99m}Tc]Tc-AC12-GGGC (11.0 ± 0.5) was observed. Importantly, tumour-to-liver ratio of [^{99m}Tc]Tc-SYNT-179 amounted to 5.9 ± 0.8, which was significantly ($p < 0.05$) higher than for other radioconjugates. Tumour-to-bone ratio was significantly ($p < 0.05$) higher for [^{99m}Tc]Tc-SYNT-179 (280.5 ± 50.8) than for [^{99m}Tc]Tc-AC12-GGGC (43.6 ± 5.7). Taking this into account, [^{99m}Tc]Tc-SYNT-179 showed the best biodistribution profile and was selected for further *in vivo* studies.

Biodistribution experiment in nude mice bearing human cancer xenografts demonstrated that the uptake of [^{99m}Tc]Tc-SYNT179 in B7-H3-positive SKOV-3 xenografts was significantly ($p < 5 \times 10^{-5}$) higher than in B7-H3-negative Ramos xenografts 4 h after injection (Fig. 5), demonstrating B7-H3-dependent accumulation in tumour.

Table 5
Biodistribution of ^{99m}Tc-labelled Affibody molecules in BALB/C nu/nu mice bearing SKOV-3 xenografts 4 h after injection. Data are expressed as the percentage of injected dose of the probe per gram of tissue (% ID/g). The data are presented as the average (n = 4) ± SD.

Site	SYNT-177	SYNT-179	SYNT-181	AC12-GGGC
Blood	0.18 ± 0.04	0.06 ± 0.01[d]	0.13 ± 0.03[d]	0.10 ± 0.01
Salivary gland	0.96 ± 0.23[a,c]	0.08 ± 0.01[a,d]	0.42 ± 0.04[d,f]	0.15 ± 0.03[c,f]
Lung	0.33 ± 0.03[a]	0.12 ± 0.01[a,d]	0.30 ± 0.07[d,f]	0.14 ± 0.03[f]
Liver	2.82 ± 0.56[a]	0.26 ± 0.02[a,d,e]	1.27 ± 0.31[d]	2.57 ± 0.42[e]
Spleen	0.62 ± 0.20[a]	0.11 ± 0.01[a,d,e]	0.59 ± 0.11[d]	0.63 ± 0.11[e]
Pancreas	0.14 ± 0.03[a]	0.05 ± 0.01[a,d]	0.13 ± 0.01[d,f]	0.06 ± 0.01[f]
Stomach	0.99 ± 0.21[a,c]	0.13 ± 0.02[a,d]	0.28 ± 0.01[d]	0.20 ± 0.05[c]
Small int	0.27 ± 0.06	0.17 ± 0.01	0.22 ± 0.07	0.16 ± 0.03
Kidney	7.90 ± 1.42	10.37 ± 1.34[d]	5.85 ± 0.28[d,f]	10.30 ± 1.13[f]
Tumour	2.15 ± 1.01	1.54 ± 0.19[d]	3.19 ± 0.21[d,f]	1.04 ± 0.08[f]
Muscle	0.03 ± 0.01	0.02 ± 0.01	0.02 ± 0.01	0.014 ± 0.004
Bone	0.02 ± 0.01[a]	0.006 ± 0.001[a,d,e]	0.018 ± 0.005[d]	0.024 ± 0.002[e]
Lower GI tract**	1.95 ± 0.28	1.47 ± 0.08	4.18 ± 0.53	1.37 ± 0.29
Body**	2.57 ± 1.22	0.61 ± 0.04	1.98 ± 0.84	1.39 ± 0.28

ANOVA test (Bonferroni's multiple comparisons test) was performed to test significant difference.
** Data for lower gastrointestinal (GI) tract with content and body are presented as % of injected dose per whole sample.
[a] Significant difference ($p < 0.05$) between [^{99m}Tc]Tc-SYNT-177 and [^{99m}Tc]Tc-SYNT-179;
[b] Significant difference ($p < 0.05$) between [^{99m}Tc]Tc-SYNT-177 and [^{99m}Tc]Tc-SYNT-181 (no significant difference);
[c] Significant difference ($p < 0.05$) between [^{99m}Tc]Tc-SYNT-177 and [^{99m}Tc]Tc-AC12-GGGC;
[d] Significant difference ($p < 0.05$) between [^{99m}Tc]Tc-SYNT-179 and [^{99m}Tc]Tc-SYNT-181;
[e] Significant difference ($p < 0.05$) between [^{99m}Tc]Tc-SYNT-179 and [^{99m}Tc]Tc-AC12-GGGC;
[f] Significant difference ($p < 0.05$) between [^{99m}Tc]Tc-SYNT-181 and [^{99m}Tc]Tc-AC12-GGGC.

Biodistribution and tumour-to-organ ratios data for [^{99m}Tc]Tc-SYNT-179 2 and 4 h after injection are presented in Fig. 6. The clearance from blood and normal organs and tissues such as salivary glands, lung, pancreas, stomach, muscle and bone was very rapid over time. Tumour uptake amounted to 4.56 ± 0.50 %ID/g already 2 h after injection followed by a decrease to 1.54 ± 0.19 %ID/g 4 h after injection. A significant difference ($p < 0.05$) in renal-associated activity was observed for 2 h (18.30 ± 3.39 %ID/g) compared to 4 h after injection (10.37 ± 1.34 %ID/g). Tumour-to-bone and tumour-to-muscle ratios were significantly ($p < 0.05$) higher at 4 h (280.5 ± 50.8 and 152.9 ± 85.8, respectively) compared to 2 h (19.8 ± 3.3 and 62.3 ± 9.8, respectively) after injection. Tumour-to-liver ratio was high at both time points of the study and no significant difference was observed at 2 (5.0 ± 0.6) and 4 h (5.9 ± 0.8) after injection.

Results of nanoSPECT/CT imaging (Fig. 7) demonstrated that visualization of B7-H3 expression in B7-H3-expressing SKOV-3 tumours using all radioconjugates was feasible at 4 h after injection. A lower accumulation of activity was visualized in liver resulting in higher tumour-to-liver signal for [^{99m}Tc]Tc-SYNT-179 (Fig. 7B), which was in agreement with the *ex vivo* biodistribution results. Activity uptake in B7-H3-negative Ramos xenografts (Fig. 8) was appreciably lower than in the B7-H3-positive SKOV-3 xenograft (Fig. 7) for all variants, which confirmed B7-H3-mediated binding *in vivo*.

Table 6
Tumour-to-organ ratios of ^{99m}Tc-labelled Affibody molecules in BALB/C nu/nu mice bearing SKOV-3 xenografts 4 h after injection. Data are expressed as the percentage of administered activity (injected probe) per gram of tissue (% ID/g). The data are presented as the average (n = 4) ± SD.

Site	SYNT-177	SYNT-179	SYNT-181	AC12-GGGC
Blood	11.3 ± 4.2[a]	25.7 ± 2.5[a,e]	23.5 ± 6.2[f]	11.0 ± 0.5[e,f]
Salivary gland	2.3 ± 1.0[a,b]	19.1 ± 4.0[a,d,e]	7.4 ± 0.4[b,d]	7.1 ± 1.8[e]
Lung	6.2 ± 2.7	12.5 ± 1.1[e]	10.4 ± 1.9[f]	7.6 ± 1.8[e,f]
Liver	0.8 ± 0.4[a,b]	5.9 ± 0.8[a,d,e]	2.6 ± 0.5[b,d,f]	0.4 ± 0.1[e,f]
Spleen	3.5 ± 1.4[a]	14.3 ± 2.8[a,d,e]	5.5 ± 0.7[d,f]	1.7 ± 0.3[e,f]
Pancreas	14.4 ± 5.4	29.9 ± 7.0	24.0 ± 1.9	17.3 ± 3.4
Stomach	2.1 ± 0.9[a,b]	12.0 ± 2.0[a,e]	11.1 ± 0.7[b,f]	5.9 ± 1.6[e,f]
Small int	7.8 ± 3.5	9.0 ± 2.1	14.3 ± 3.6	6.5 ± 1.1
Kidney	0.3 ± 0.1	0.15 ± 0.01[d]	0.55 ± 0.04[d,f]	0.10 ± 0.01[f]
Muscle	46.2 ± 14.6	152.9 ± 85.8	203.1 ± 92.0	72.2 ± 20.8
Bone	131.8 ± 56.4	280.5 ± 50.8[d,e]	183.5 ± 39.7[d,f]	43.6 ± 5.7[e,f]

ANOVA test (Bonferroni's multiple comparisons test) was performed to test significant difference.
[a] Significant difference ($p < 0.05$) between [^{99m}Tc]Tc-SYNT-177 and [^{99m}Tc]Tc-SYNT-179;
[b] Significant difference ($p < 0.05$) between [^{99m}Tc]Tc-SYNT-177 and [^{99m}Tc]Tc-SYNT-181;
[c] Significant difference ($p < 0.05$) between [^{99m}Tc]Tc-SYNT-177 and [^{99m}Tc]Tc-AC12-GGGC (no significant difference);
[d] Significant difference ($p < 0.05$) between [^{99m}Tc]Tc-SYNT-179 and [^{99m}Tc]Tc-SYNT-181;
[e] Significant difference ($p < 0.05$) between [^{99m}Tc]Tc-SYNT-179 and [^{99m}Tc]Tc-AC12-GGGC;
[f] Significant difference ($p < 0.05$) between [^{99m}Tc]Tc-SYNT-181 and [^{99m}Tc]Tc-AC12-GGGC.

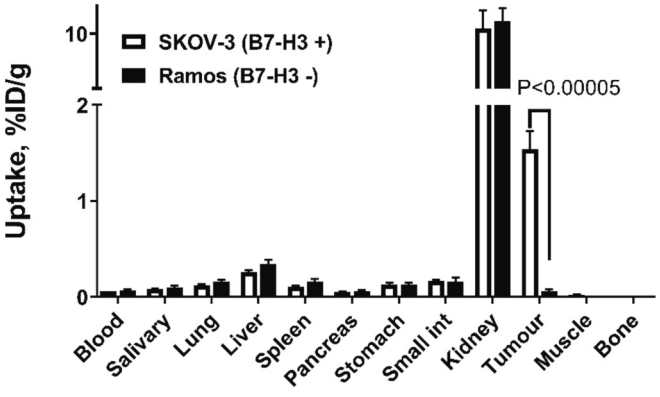

Fig. 5. Uptake of [^{99m}Tc]Tc-SYNT-179 in SKOV-3 (B7-H3-positive) and Ramos (B7-H3-negative) xenografts 4 h after injection. Data are expressed as %ID/g and average from four mice ± SD. Unpaired *t*-test was used to obtain p-value.

4. Discussion

Radionuclide molecular imaging of B7-H3 expression might be used for stratification of patients for B7-H3-targeting therapies. The feasibility of *in vivo* imaging of B7-H3 immune checkpoint molecule using Affibody molecule has been demonstrated recently [47]. However, the tumour uptake of the AC12 Affibody molecule labelled with ^{99m}Tc in B7-H3-expressing xenograft needed to be improved in order to obtain higher imaging contrast. An improvement in binding affinity of Affibody molecules to B7-H3 target would be an option. Dimerization and affinity

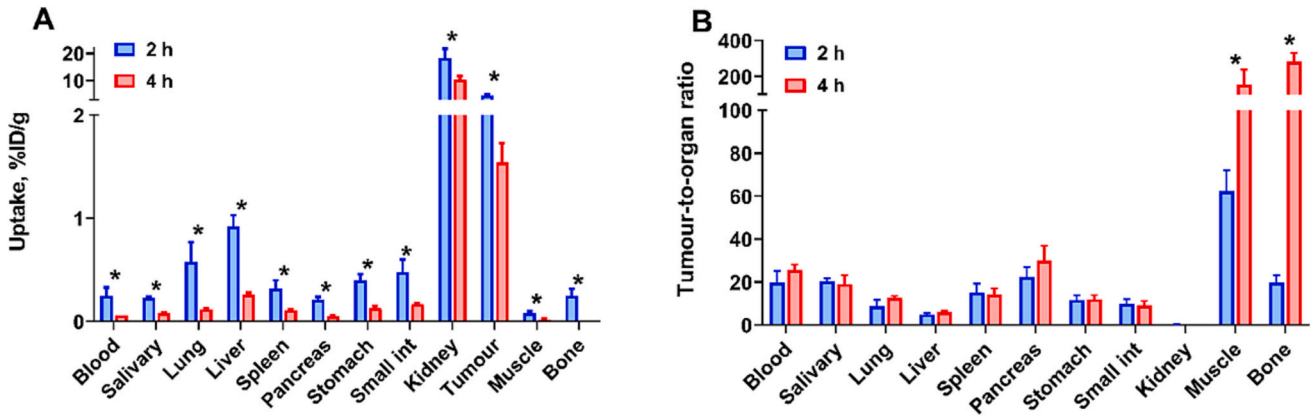

Fig. 6. (A) Biodistribution and (B) tumour-to-organ ratios of [^{99m}Tc]Tc-SYNT-179 in BALB/C nu/nu mice bearing SKOV-3 xenografts 2 and 4 h after injection. Data are expressed as the percentage injected dose of probe per gram of tissue (% ID/g). The data are presented as the average (n = 4) ± SD. The significance indicator (*) corresponds to $p < 0.05$ in an unpaired t-test.

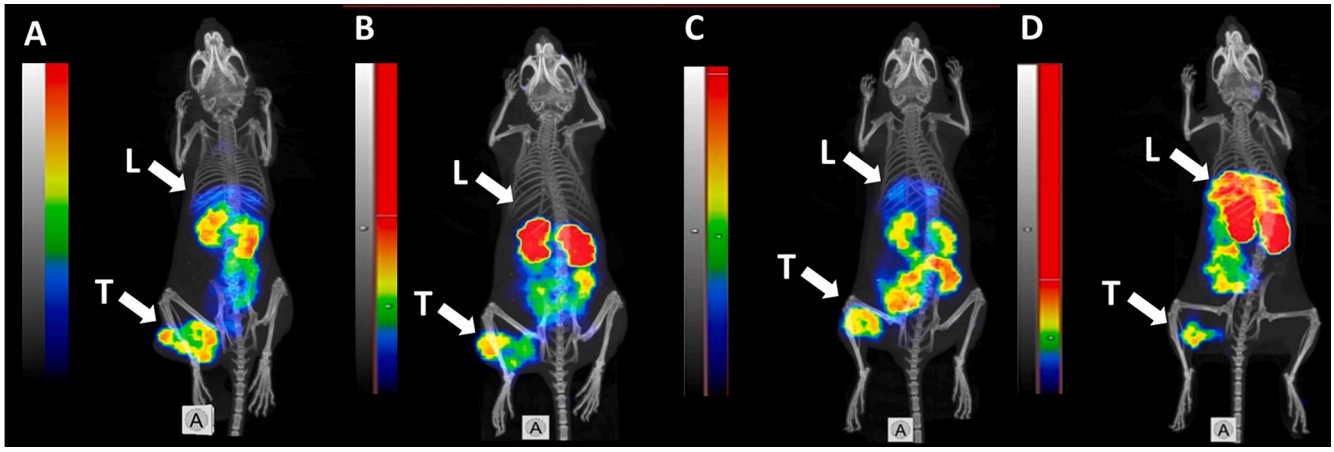

Fig. 7. Imaging of (A) [^{99m}Tc]Tc-SYNT-177, (B) [^{99m}Tc]Tc-SYNT-179, (C) [^{99m}Tc]Tc-SYNT-181 and (D) [^{99m}Tc]Tc-AC12-GGGC in BALB/C nu/nu mice bearing B7-H3-positive SKOV-3 xenografts 4 h after injection (maximum intensity projections). Linear relative scale (arbitrary units normalized to a maximum count rate) is provided for each image. Scales were adjusted to show red pixels in xenografts. 3 μg of labelled Affibody molecule (6 MBq, 100 μL in PBS) was injected into the tail vein. Arrows point at tumour (T) and liver (L). (For interpretation of the references to color in this figure legend, the reader is referred to the web version of this article.)

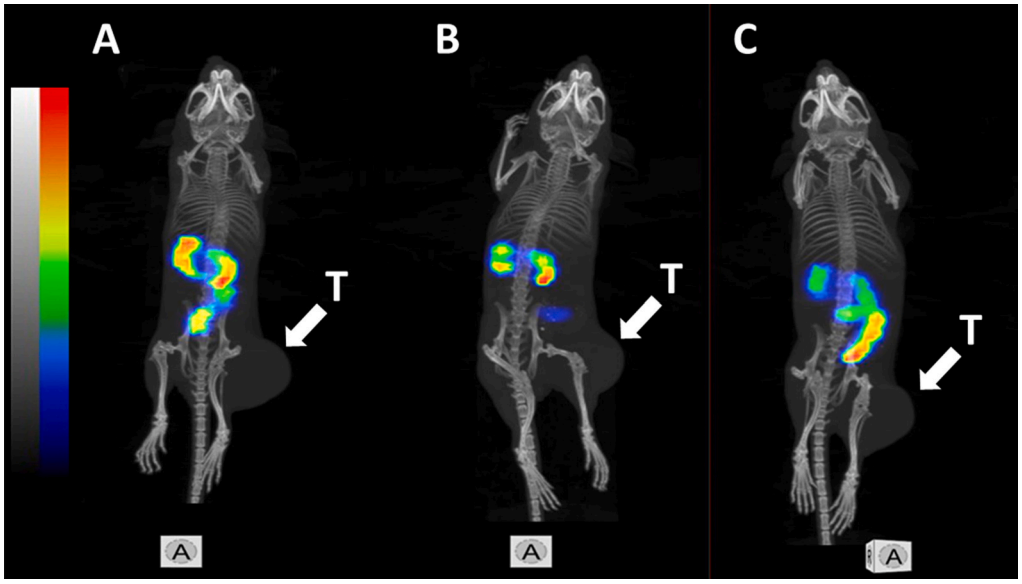

Fig. 8. Imaging of (A) [^{99m}Tc]Tc-SYNT-177, (B) [^{99m}Tc]Tc-SYNT-179 and (C) [^{99m}Tc]Tc-SYNT-181 in BALB/C nu/nu mice bearing Ramos (B7-H3-negative) xenografts 4 h after injection (maximum intensity projections). The same linear relative scale (arbitrary units normalized to a maximum count rate) is applied for each image. 3 μg of labelled Affibody molecule (6 MBq, 100 μL in PBS) was injected into the tail vein. Arrows point at tumours (T). Imaging of [^{99m}Tc]Tc-AC12-GGGC on Ramos xenograft was performed previously [47].

maturation are the possible strategies to improve affinity of Affibody molecules to the target. Previous studies with HER2-targeting Affibody molecules demonstrated that keeping the size small might be more important than gaining functional affinity by dimerization [29,51]. Thus, an affinity maturation of the AC12 Affibody molecule, as a method to improve binding strength of anti-B7-H3 Affibody molecules to B7-H3 target, was utilized and generated candidates that were assessed in this study.

The improvement in detectors and software makes SPECT/CT an increasingly attractive imaging modality in the clinic with less costly SPECT cameras than PET scanners [52,53]. Amongst possible radionuclides for SPECT imaging, generator-produced technetium-99m (^{99m}Tc) with optimal half-life ($T_{1/2}$ = 6 h), excellent availability, less costly production, favourable emitted photon energy for SPECT cameras (E_γ = 140.5 keV), and low absorbed-dose burden to the patient is the most commonly used radionuclide in nuclear medicine [54]. It should be noted that the stability of ^{99m}Tc-labelled conjugates is crucial to prevent the dissociation of free radionuclide in blood and healthy organs and tissues and an increased background signal. The labelling chemistry of Affibody molecules labelled with ^{99m}Tc was well-studied particularly using peptide-based chelators [27,28]. ^{99m}Tc has shown a high thiol-affinity, which enables stable complex with short peptide sequences incorporating a thiol-containing moiety from *e.g.* cysteine [55]. Earlier studies have shown that Affibody molecules targeting different molecular targets such as the anti-HER2 ZHER2 [30,55,56], anti-EGFR ZEGFR:2377 [27,28] and anti-B7-H3 Affibody molecules [47] can be stably labelled using peptide-based cysteine-containing chelators. It was found that composition of peptide-based chelators and their position at Affibody molecules could modulate targeting properties of the ^{99m}Tc label, its retention in excretory organs, excretion pathway and overall biodistribution of ^{99m}Tc-labelled Affibody molecules [28,56–58]. According to the previous study [57], the best imaging contrast has been obtained by using an Affibody molecule containing a –GGGC chelator at the C-terminus for targeting HER2-expressing tumours. Importantly, previous studies have demonstrated that –GGGC provided very stable coupling of ^{99m}Tc [30,57,59] and ^{188}Re [60,61] to Affibody molecules. Thus, a –GGGC chelator was selected for labelling of anti B7-H3 Affibody molecules with ^{99m}Tc in this study. Three variants of affinity matured Affibody molecules containing a –GGGC amino acid sequence at the C-terminus for labelling with ^{99m}Tc were synthesized.

Labelling with ^{99m}Tc was performed with high efficiency. No release of activity from the Affibody molecule was observed after 1-h incubation in excess of PBS at 37 °C (Table 3). Binding to two B7-H3-expressing cell lines was highly B7-H3-specific *in vitro* (Fig. 3).

The results of the LigandTracer measurements of the matured radiolabelled Affibody molecules showed that there are two different interactions of ^{99m}Tc-labelled conjugates with B7-H3 on living cells, which might be explained by structure of B7-H3 molecule [62]. B7-H3 have several epitopes, located on different subunits, with the same amino acid composition, but the steric hindrance might be different for different epitope locations. Thus, affinities to different epitopes might be different. Both the K_{D1} and the K_{D2} values for all three new variants were appreciably lower than for the parental variant [^{99m}Tc]Tc-AC12-GGGC, *i.e.* their affinity was higher (Table 4 and Fig. 4). [^{99m}Tc]Tc-SYNT-179 showed the highest overall affinity value with K_{D1} (K_{D1} = 0.028 ± 0.001 nM). The affinity of the most abundant interaction was improved 5.3–8.2-fold. This correlates with the EC_{50} values derived from the nonradioactive cell-based experiments.

Several studies have demonstrated that minor changes (even 2–3 amino acids) in composition of amino acids within the binding site of Affibody molecules can noticeably influence their off-target interactions (including binding to blood proteins) and consequently their biodistribution profile [28,34,43,63,64]. Biodistribution data in tumour-bearing mice 4 h after injection (Table 4) demonstrated that [^{99m}Tc]Tc-SYNT-179 showed the lowest blood concentration and lower uptake in all organs and tissues. The hepatic uptake of [^{99m}Tc]Tc-SYNT-179 was significantly lower than for the other conjugates. Particularly, it was 10-fold lower than for [^{99m}Tc]Tc-AC12-GGGC 4 h after injection. Previous studies with other Affibody molecules have demonstrated that substitution of amino acids with hydrophobic side chains by amino acids with hydrophilic ones often resulted in more rapid excretion from blood and reduced hepatic uptake [28,58]. In new Affibody variants (Fig. 9), a hydrophobic alanine was replaced with hydrophilic asparagine (SYNT-179) or charged lysine (SYNT-177 and SYNT-181). In addition, a methionine was replaced by lysine. Still, the reduction of the hepatic uptake of [^{99m}Tc]Tc- SYNT-177 and [^{99m}Tc]Tc-SYNT-181 was moderate at the best. A major difference between SYNT-179 and other variants is a substitution of a glycine by aspartate. This is in agreement with the previous data, showing that incorporation of negatively charged amino acids is associated with lower uptake in liver [28,58].

A sufficient tumour uptake and low uptake in normal organs and tissues resulted in higher tumour-to-organ ratios for [^{99m}Tc]Tc-SYNT-179 than for other variants (Table 6). Tumour-to-organ ratios except tumour-to-pancreas, tumour-to-small intestine and tumour-to-muscle were significantly ($p < 0.05$) higher for [^{99m}Tc]Tc-SYNT-179 than those for [^{99m}Tc]Tc-AC12-GGGC. Significantly higher tumour-to-liver ratio for [^{99m}Tc]Tc-SYNT-179 (5.9 ± 0.8) than for the reference variant [^{99m}Tc]Tc-AC12-GGGC (0.41 ± 0.07) was observed. Tumour-to-liver and tumour-to-bone ratios were 6- and 15-fold higher for [^{99m}Tc]Tc-SYNT-179 than those for [^{99m}Tc]Tc-AC12-GGGC, respectively, which are very important for detection of hepatic and bone metastases at early time point of imaging. Another interesting observation in this study is the difference in the renal uptake of different variants of B7-H3-targeting Affibody molecules (Table 5). A number of previous studies have demonstrated that the use of the sequence –GGGC for labelling with ^{99m}Tc or ^{188}Re resulted in a non-residualizing label, which is "leaking" from cells after internalization and proteolytic degradation of targeting proteins [30,57,60]. This resulted in a rapid release of activity from kidneys, where Affibody molecules are rapidly internalized and degraded after binding to scavenger receptors in proximal tubuli. However, experience with radioiodine-based non-residualizing labels shows that the renal retention might be different depending on the composition of Affibody molecules [34]. A possible explanation is that the different amino acid compositions of proteins confer different susceptibility to endopeptidases in lysosomes, influencing the lysosomal degradation rate and, in this way, the rate of activity release from kidneys.

SPECT/CT imaging (Figs. 7 and 8) confirmed the biodistribution results. Taking this into account, the affinity matured SYNT-179 Affibody molecule labelled with ^{99m}Tc with improved affinity to B7-H3 target provided better biodistribution and targeting properties for imaging of B7-H3-expressing tumours compared to [^{99m}Tc]Tc-AC12-GGGC. Based on the biodistribution results, it was concluded that [^{99m}Tc]Tc-SYNT-179 was the best candidate.

The uptake of [^{99m}Tc]Tc-SYNT-179 in B7-H3-positive SKOV-3 xenografts was 25-fold higher than in B7-H3-negative Ramos xenografts (Fig. 6), which clearly demonstrates B7-H3-specific targeting *in vivo*.

Biodistribution of [^{99m}Tc]Tc-AC12-GGGC was previously studied at 2 h after injection [47]. Comparison of the earlier measured biodistribution of [^{99m}Tc]Tc-AC12-GGGC with the biodistribution of [^{99m}Tc]Tc-SYNT-179 demonstrated that tumour uptake was 2.2-fold higher for [^{99m}Tc]Tc-SYNT-179 (4.56 ± 0.50 %ID/g) than for [^{99m}Tc]Tc-AC12-GGGC (2.11 ± 0.46 %ID/g) at 2 h after injection. Low uptake in almost all organs and tissues at 2 h after injection resulted in appreciably higher tumour-to-organ ratios for [^{99m}Tc]Tc-SYNT-179 than for [^{99m}Tc]Tc-AC12-GGGC.

Tumour-to-blood and tumour-to-liver ratios were 2.4- and 7.7-fold higher than those for [^{99m}Tc]Tc-AC12-GGGC at 2 h after injection. Interestingly, the tumour uptake for [^{99m}Tc]Tc-SYNT-179 (4.56 ± 0.50 %ID/g) only 2 h after injection was at the same level as for an anti-B7-H3 humanized monoclonal antibody labelled with zirconium-89 (^{89}Zr-DS-5573a) (4.58 ± 0.69 %ID/g) [18] used for preclinical imaging of B7-H3

Fig. 9. Alignment of evaluated Affibody molecules.

in MDA-MB-231 tumours at the day of injection. However, the uptake in blood and all organs and tissues such as liver, kidneys and bone of ^{89}Zr-DS-5573a was appreciably higher at the day of injection. Taking this into account, affinity maturation to improve affinity and increase tumour uptake of the anti-B7-H3 Affibody molecules improved their biodistribution and targeting properties for imaging of B7-H3-expressing tumours. [^{99m}Tc]Tc-SYNT-179 provided the best biodistribution and targeting properties for preclinical imaging of B7-H3 at day of injection, which was appreciably improved compared to the parental AC12-GGGC Affibody molecule.

This study demonstrated that there was a release of activity from tumours between 2 and 4 h after injection of [^{99m}Tc]Tc-SYNT-179 (Fig. 6A). Although affinity maturation has appreciably increased the strength of binding to B7-H3, the most abundant interaction of [^{99m}Tc]Tc-SYNT-179 with human B7-H3 remained to be in a single digit nanomolar range. This improved its tumour retention compared to [^{99m}Tc]Tc-AC12-GGGC. However, such increase might not be sufficient to prevent dissociation of [^{99m}Tc]Tc-SYNT-179 from the target *in vivo* and its release from tumours completely, when the expression is on the level of 45,000–60,000 molecules per cell [43]. Still, there was a simultaneous clearance of activity from normal tissues. Thus, tumour-to-organ ratios did not change significantly between 2 and 4 h after injection. The only exception was a significant ($p < 0.05$) increase of tumour-to-muscle and tumour-to-bone ratios by 4 h after injection. Both bone and muscle are tissues often harbouring or surrounding metastatic lesions for many malignancies and an increase of tumour-to-muscle and tumour-to-bone ratios by 4 h would facilitate detection of small metastases due to the increased imaging contrast. On the other hand, decrease of the tumour uptake by 4 h might require either longer scanning time or increase of injected activity to ensure that a counting statistics would be sufficient for a high fidelity reconstruction of images. Still, the tumour-to-bone and tumour-to-muscle ratios at 2 h (19.8 ± 3.3 and 62.3 ± 9.8, respectively) are high enough, and this time point might be close to optimum. Apparently, future clinical studies should address the issue of a selection of the optimal time point for imaging using [^{99m}Tc]Tc-SYNT-179.

5. Conclusions

In conclusion, the procedure used for affinity maturation resulted in an increased affinity by 5–8-fold through an affinity maturation step for SYNT-179 compared to AC12. SYNT-179 could be a promising candidate for aiming at clinical application in the future.

Funding

This research was funded by the grants from Swedish Cancer Society (Cancerfonden, grants 20 0815, 21 1485 Pj), Swedish Research Council (Vetenskapsrådet, grants VR 2019-00986 and 2019-00994) and Ministry of Science and Higher Education (075-15-2022-1103), Personal post-doctoral grant from Uppsala University (UFV-PA 2022/3323).

Institutional review board statement

Animal studies were planned in agreement with EU Directive 2010/63/EU for animal experiments and Swedish national legislation concerning protection of laboratory animals and were approved by the Ethics Committee for Animal Research in Uppsala, Sweden (ethical permission C4/16).

Informed consent statement

Not applicable.

CRediT authorship contribution statement

Conceptualization, F.Y.F., V.T. and M.O. Methodology, F.Y.F., A.O., V.T., M.O. Formal analysis, M.O., E.A.B. and V.T. Investigation, M.O., E.A.B., T.X.,Y.L., E.V.P.,S.K., I.K., E.R., V.T., F.Y.F. and A.O. Resources, V.T., F.Y.F. and A.O. Data curation, V.T. and M.O. Writing—original draft preparation, M.O. Writing—review and editing, M.O., E.A.B., T.X., Y.L., E.V.P., I.K., E.R., V.T., F.Y.F. and A.O. Visualization, A.O. Supervision, V.T., F.Y.F. and A.O. Project administration, V.T., F.Y.F. and A.O. Funding acquisition, V.T. All authors have read and agreed to the published version of the manuscript.

Declaration of competing interest

V.T., and A.O. are minority shareholders (own stock) in Affibody AB. M.O., S. K., I.K., E.R., and F.Y.F., are employees of Affibody AB. E.A.B., T.X., Y.L., and E.P., declare no potential conflict of interest. The funders had no role in the design of the study, in the collection, analyses, or interpretation of data, in the writing of the manuscript, or in the decision to publish the results.

Data availability statement

Data is contained within the article or supplementary material.

Acknowledgments

This research was funded by the grants from Swedish Cancer Society (Cancerfonden, grants 20 0815, 21 1485 Pj), Swedish Research Council (Vetenskapsrådet, grants VR 2019-00986 and 2019-00994) and Ministry of Science and Higher Education (075-15-2022-1103), Personal post-doctoral grant from Uppsala University (UFV-PA 2022/3323).

References

[1] Zhou WT, Jin WL. B7-H3/CD276: an emerging cancer immunotherapy. Front Immunol 2021;12:2021.
[2] Pulido R, Nunes-Xavier CE. Hopes on immunotherapy targeting B7-H3 in neuroblastoma. Transl Oncol 2023;27:101580.
[3] Wang J, Chong KK, Nakamura Y, Nguyen L, Huang SK, Kuo C, et al. B7-H3 associated with tumor progression and epigenetic regulatory activity in cutaneous melanoma. J Invest Dermatol 2013;133:2050–8.
[4] Lemke D, Pfenning PN, Sahm F, Klein AC, Kempf T, Warnken U, et al. Costimulatory protein 4IgB7H3 drives the malignant phenotype of glioblastoma by mediating immune escape and invasiveness. Clin Cancer Res 2012;18:105–17.
[5] Li F, Chen H, Wang D. Silencing of CD276 suppresses lung cancer progression by regulating integrin signaling. J Thorac Dis 2020;12:2137–45.
[6] Yamato I, Sho M, Nomi T, Akahori T, Shimada K, Hotta K, et al. Clinical importance of B7-H3 expression in human pancreatic cancer. Br J Cancer 2009;101:1709–16.
[7] Inamura K, Takazawa Y, Inoue Y, Yokouchi Y, Kobayashi M, Saiura A, et al. Tumor B7-H3 (CD276) expression and survival in pancreatic cancer. J Clin Med 2018;7:172.

[8] Cong F, Yu H, Gao X. Expression of CD24 and B7-H3 in breast cancer and the clinical significance. Oncol Lett 2017;14:7185–90.
[9] Zang X, Thompson RH, AlAhmadie HA, Serio AM, Reuter VE, Eastham JA, et al. B7-H3 and B7x are highly expressed in human prostate cancer and associated with disease spread and poor outcome. Proc Natl Acad Sci U S A 2007;104:19458–63.
[10] Roth TJ, Sheinin Y, Lohse CM, Kuntz SM, Frigola X, Inman BA, et al. B7-H3 ligand expression by prostate cancer: a novel marker of prognosis and potential target for therapy. Cancer Res 2007;67:7893–900.
[11] Zang X, Sullivan PS, Soslow RA, Waitz R, Reuter VE, Wilton A, et al. Tumor associated endothelial expression of B7-H3 predicts survival in ovarian carcinomas. Mod Pathol 2010;23:1104–12.
[12] Modak S, Kramer K, Gultekin SH, Guo HF, Cheung NK. Monoclonal antibody 8H9 targets a novel cell surface antigen expressed by a wide spectrum of human solid tumors. Cancer Res 2001;61:4048–54.
[13] Ingebrigtsen VA, Boye K, Tekle C, Nesland JM, Flatmark K, Fodstad Ø. B7-H3 expression in colorectal cancer: nuclear localization strongly predicts poor outcome in colon cancer. Int J Cancer 2012;131:2528–36.
[14] Yuan H, Wei X, Zhang G, Li C, Zhang X, Hou J. B7-H3 over expression in prostate cancer promotes tumor cell progression. J Urol 2011;186:1093–9.
[15] Sun T-W, Gao Q, Qiu S-J, Zhou J, Wang X-Y, Yi Y, et al. B7-H3 is expressed in human hepatocellular carcinoma and is associated with tumor aggressiveness and postoperative recurrence. Cancer Immunol Immunother 2012;61:2171–82.
[16] Wang L, Zhang Q, Chen W, Shan B, Ding Y, Zhang G, et al. B7-H3 is overexpressed in patients suffering osteosarcoma and associated with tumor aggressiveness and metastasis. PloS One 2013;8:e70689.
[17] Salih S, Elliyanti A, Alkatheeri A, AlYafei F, Almarri B, Khan H. The role of molecular imaging in personalized medicine. J Pers Med 2023;13:369.
[18] Burvenich IJG, Parakh S, Lee F-T, Guo N, Liu Z, Gan HK, et al. Molecular imaging of T cell co-regulator factor B7-H3 with 89Zr-DS-5573a. Theranostics. 2018;8:4199–209.
[19] Kasten BB, Gangrade A, Kim H, Fan J, Ferrone S, Ferrone CR, et al. ^{212}Pb-labeled B7-H3-targeting antibody for pancreatic cancer therapy in mouse models. Nucl Med Biol 2018;58:67–73.
[20] Modak S, Zanzonico P, Grkovski M, Slotkin EK, Carrasquillo JA, Lyashchenko SK, et al. B7H3-directed intraperitoneal radioimmunotherapy with radioiodinated ombur-tamab for desmoplastic small round cell tumor and other peritoneal tumors: results of a phase I study. J Clin Oncol 2020;38:4283–91.
[21] Kramer K, Pandit-Taskar N, Kushner BH, Zanzonico P, Humm JL, Tomlinson U, et al. Phase 1 study of intraventricular ^{131}I-omburtamab targeting B7H3 (CD276)-expressing CNS malignancies. J Hematol Oncol 2022;15:165.
[22] Wu AM. Engineered antibodies for molecular imaging of cancer. Methods. 2014;65:139–47.
[23] Freise AC, Wu AM. In vivo imaging with antibodies and engineered fragments. Mol Immunol 2015;67:142–52.
[24] Even AJ, Hamming-Vrieze O, van Elmpt W, Winnepenninckx VJ, Heukelom J, Tesselaar ME, et al. Quantitative assessment of zirconium-89 labeled cetuximab using PET/CT imaging in patients with advanced head and neck cancer: a theragnostic approach. Oncotarget. 2017;8:3870–80.
[25] Ståhl S, Gräslund T, Eriksson Karlström A, Frejd FY, Nygren P-Å, Löfblom J. Affibody molecules in biotechnological and medical applications. Trends Biotechnol 2017;35:691–712.
[26] Krasniqi A, D'Huyvetter M, Devoogdt N, Frejd FY, Sörensen J, Orlova A, et al. Same-day imaging using small proteins: clinical experience and translational prospects in oncology. J Nucl Med 2018;59:885–91.
[27] Andersson KG, Oroujeni M, Garousi J, Mitran B, Ståhl S, Orlova A, et al. Feasibility of imaging of epidermal growth factor receptor expression with ZEGFR:2377 affibody molecule labeled with ^{99m}Tc using a peptide-based cysteine-containing chelator. Int J Oncol 2016;49:2285–93.
[28] Oroujeni M, Andersson KG, Steinhardt X, Altai M, Orlova A, Mitran B, et al. Influence of composition of cysteine-containing peptide-based chelators on biodistribution of ^{99m}Tc-labeled anti-EGFR affibody molecules. Amino Acids 2018;50:981–94.
[29] Orlova A, Magnusson M, Eriksson TLJ, Nilsson M, Larsson B, Höidén-Guthenberg I, et al. Tumor imaging using a picomolar affinity HER2 binding affibody molecule. Cancer Res 2006;66:4339–48.
[30] Oroujeni M, Rinne SS, Vorobyeva A, Loftenius A, Feldwisch J, Jonasson P, et al. Preclinical evaluation of ^{99m}Tc-ZHER2:41071, a second-generation Affibody-based HER2-visualizing imaging probe with a low renal uptake. Int J Mol Sci 2021;22:2770.
[31] Rosestedt M, Andersson KG, Mitran B, Tolmachev V, Löfblom J, Orlova A, et al. Affibody-mediated PET imaging of HER3 expression in malignant tumours. Sci Rep 2015;5:15226.
[32] Strand J, Varasteh Z, Eriksson O, Abrahmsen L, Orlova A, Tolmachev V. Gallium-68-labeled affibody molecule for PET imaging of PDGFRbeta expression in vivo. Mol Pharm 2014;11:3957–64.
[33] Liu Y, Yu S, Xu T, Bodenko V, Orlova A, Oroujeni M, et al. Preclinical evaluation of a new format of ^{68}Ga- and ^{111}In-labeled Affibody molecule ZIGF-1R:4551 for the visualization of IGF-1R expression in malignant tumors using PET and SPECT. Pharmaceutics. 2022;14:1475.
[34] Garousi J, Honarvar H, Andersson KG, Mitran B, Orlova A, Buijs J, et al. Comparative evaluation of Affibody molecules for radionuclide imaging of in vivo expression of carbonic anhydrase IX. Mol Pharm 2016;13:3676–87.
[35] Sörensen J, Sandberg D, Sandström M, Wennborg A, Feldwisch J, Tolmachev V, et al. First-in-human molecular imaging of HER2 expression in breast cancer metastases using the ^{111}In-ABY-025 Affibody molecule. J Nucl Med 2014;55:730–5.
[36] Sörensen J, Velikyan I, Sandberg D, Wennborg A, Feldwisch J, Tolmachev V, et al. Measuring HER2-receptor expression in metastatic breast cancer using [^{68}Ga]ABY-025 Affibody PET/CT. Theranostics. 2016;6:262–71.
[37] Alhuseinalkhudhur A, Lindman H, Liss P, Sundin T, Frejd FY, Hartman J, et al. HER2-targeting [^{68}Ga]Ga-ABY-025 PET predicts early metabolic response in breast cancer patients - results from a Phase II study. J Nucl Med 2023: jnumed.122.265364. https://doi.org/10.2967/jnumed.122.265364 [Epub ahead of print].
[38] Wållberg H, Orlova A. Slow internalization of anti-HER2 synthetic affibody monomer ^{111}In-DOTA-ZHER2:342-pep2: implications for development of labelled tracers. Cancer Biother Radiopharm 2008;23:435–42.
[39] Tran TA, Rosik D, Abrahmsen L, Sandström M, Sjöberg A, Wållberg H, et al. Design, synthesis and biological evaluation of a multifunctional HER2-specific Affibody molecule for molecular imaging. Eur J Nucl Med Mol Imaging 2009;36:1864–73.
[40] Adams GP, Schier R, Marshall K, Wolf EJ, McCall AM, Marks JD, et al. Increased affinity leads to improved selective tumor delivery of single-chain Fv antibodies. Cancer Res 1998;58:485–90.
[41] Adams GP, Schier R, McCall AM, Simmons HH, Horak EM, Alpaugh RK, et al. High affinity restricts the localization and tumor penetration of single-chain fv antibody molecules. Cancer Res 2001;61:4750–5.
[42] Adams GP, Tai MS, McCartney JE, Marks JD, Stafford WF, Houston LL, et al. Avidity-mediated enhancement of in vivo tumor targeting by single-chain Fv dimers. Clin Cancer Res 2006;12:1599–605.
[43] Tolmachev V, Tran TA, Rosik D, Sjöberg A, Abrahmsén L, Orlova A. Tumor targeting using Affibody molecules: interplay of affinity, target expression level, and binding site composition. J Nucl Med 2012;53:953–60.
[44] Friedman M, Orlova A, Johansson E, Eriksson TLJ, Höidén-Guthenberg I, Tolmachev V, et al. Directed evolution to low nanomolar affinity of a tumor-targeting epidermal growth factor receptor-binding affibody molecule. J Mol Biol 2008;376:1388–402.
[45] Malm M, Kronqvist N, Lindberg H, Gudmundsdotter L, Bass T, Frejd FY, et al. Inhibiting HER3-mediated tumor cell growth with Affibody molecules engineered to low picomolar affinity by position-directed error-prone PCR-like diversification. PloS One 2013;8:e62791.
[46] Lindborg M, Cortez E, Höidén-Guthenberg I, Gunneriusson E, von Hage E, Syud F, et al. Engineered high-affinity affibody molecules targeting platelet-derived growth factor receptor β in vivo. J Mol Biol 2011;407:298–315.
[47] Oroujeni M, Bezverkhniaia EA, Xu T, Liu Y, Plotnikov EV, Karlberg I, et al. Evaluation of an Affibody-based binder for imaging of immune check-point molecule B7-H3. Pharmaceutics. 2022;14:1780.
[48] Ahlgren S, Andersson KG, Tolmachev V. Kit formulation for ^{99m}Tc-labeling of recombinant anti-HER2 affibody molecules with a C-terminally engineered cysteine. Nucl Med Biol 2010;37:539–46.
[49] Björke H, Andersson KG. Automated, high-resolution cellular retention and uptake studies in vitro. Appl Radiat Isot 2006;64:901–5.
[50] Altschuh D, Björkelund H, Strandgård J, Choulier L, Malmqvist M, Andersson KG. Deciphering complex protein interaction kinetics using Interaction Map. Biochem Biophys Commun 2012;428:74–9.
[51] Tolmachev V, Friedman M, Sandström M, Eriksson TLJ, Rosik D, Hodik M, et al. Affibody molecules for epidermal growth factor receptor targeting in vivo: aspects of dimerization and labeling chemistry. JNM. 2009;50:274–83.
[52] Rahmim A, Zaidi H. PET versus SPECT: strengths, limitations and challenges. Nucl Med Commun 2008;29:193–207.
[53] Slomka PJ, Pan T, Berman DS, Germano G. Advances in SPECT and PET hardware. Prog Cardiovasc Dis 2015;57:566–78.
[54] Banerjee SR, Maresca KP, Francesconi L, Valliant J, Babich JW, Zubieta J. New directions in the coordination chemistry of ^{99m}Tc: a reflection on technetium core structures and a strategy for new chelate design. Nucl Med Biol 2005;32:1–20.
[55] Ahlgren S, Wållberg H, Tran TA, Widström C, Hjertman M, Abrahmsén L, et al. Targeting of HER2-expressing tumors with a site-specifically ^{99m}Tc-labeled recombinant affibody molecule, ZHER2:2395, with C-terminally engineered cysteine. J Nucl Med 2009;50:781–9.
[56] Altai M, Wållberg H, Orlova A, Rosestedt M, Hosseinimehr SJ, Tolmachev V, et al. Order of amino acids in C-terminal cysteine-containing peptide-based chelators influences cellular processing and biodistribution of ^{99m}Tc-labeled recombinant affibody molecules. Amino Acids 2012;42:1975–85.
[57] Wållberg H, Orlova A, Altai M, Widström C, Hosseinimehr SJ, Malmberg J, et al. Molecular design and optimization of ^{99m}Tc-labeled recombinant affibody molecules improves their biodistribution and imaging properties. J Nucl Med 2011;52:461–9.
[58] Hofström C, Altai M, Honarvar H, Strand J, Malmberg J, Hosseinimehr SJ, et al. HAHAHA, HEHEHE, HIHIHI, or HKHKHK: influence of position and composition of histidine containing tags on biodistribution of [(^{99m})Tc(CO)$_3$](+)-labeled affibody molecules. J Med Chem 2013;56:4966–74.
[59] Mitran B, Altai M, Hofström C, Honarvar H, Sandström M, Orlova A, et al. Evaluation of 99mTc-Z IGF1R:4551-GGGC affibody molecule, a new probe for imaging of insulin-like growth factor type 1 receptor expression. Amino Acids 2015;47:303–15.
[60] Altai M, Honarvar H, Wållberg H, Strand J, Varasteh Z, Rosestedt M, et al. Selection of an optimal cysteine-containing peptide-based chelator for labeling of affibody molecules with (188)Re. Eur J Med Chem 2014;87:519–28.
[61] Liu Y, Vorobyeva A, Orlova A, Konijnenberg MW, Xu T, Bragina O, et al. Experimental therapy of HER2-expressing xenografts using the second-generation HER2-targeting Affibody molecule 188Re-ZHER2:41071. Pharmaceutics. 2022;14:1092.

[62] Chen YW, Tekle C, Fodstad O. The immunoregulatory protein human B7H3 is a tumor-associated antigen that regulates tumor cell migration and invasion. Curr Cancer Drug Targets 2008;8:404–13.
[63] Tolmachev V, Hofström C, Malmberg J, Ahlgren S, Hosseinimehr SJ, Sandström M, et al. HEHEHE-tagged affibody molecule may be purified by IMAC, is conveniently labeled with [^{99m}Tc(CO)$_3$] (+) and shows improved biodistribution with reduced hepatic radioactivity accumulation. Bioconjug Chem 2010;21:2013–22.
[64] Andersson KG, Rosestedt M, Varasteh Z, Malm M, Sandström M, Tolmachev V, et al. Comparative evaluation of ^{111}In-labeled NOTA-conjugated affibody molecules for visualization of HER3 expression in malignant tumors. Oncol Rep 2015;34:1042–8.